Small scale energy release and the acceleration and transport of energetic particles

Hugh Hudson[1] and Nicole Vilmer[2]

[1] SSL/UCB Berkeley, CA USA 94720 hhudson@hhudson@ssl.berkeley.edu
[2] LESIA, Observatoire de Paris, Meudon, FR 92195 nicole.vilmer@obspm.fr

Summary. We report on results presented at the sessions of Working Group 1 at CESRA 2004, which covered the topic area of the title of this paper. The working-group participants are listed in the Appendix, and the topics discussed have been brought together in several general areas of focus. The emphasis on the discussion is from the point of view of radiophysics. We organize the material by presenting new constraints imposed by the recent high-energy and radio observations. We note though that multi-wavelength knowledge is generally vital in understanding all of the phenomena involved. The new constraints include exciting new millimeter-wave discoveries, among others. We then place these observations into the framework of our knowledge of the acceleration and propagation of high-energy particles, and of their radio emission mechanisms. The RHESSI[3] results are the most distinctive in this time frame, and they have made possible several new advances.

1 Introduction

The techniques of solar radio astronomy have historically led the way in our studies of the non-thermal behavior of the solar corona. In recent decades X-ray and EUV observations have begun to approach the resolution (the arc sec range) of the radio observations at mm/cm wavelengths (e.g. those of the VLA[4] and NoRH[5]) and we now find ourselves in a happy era in which these very different wave bands can all contribute to our understanding.

This article discusses material presented in the CESRA 2004 working-group sessions on the subject named in the title of this chapter; please see the CESRA 2001 proceedings [1] for continuity. Although we deal with multi-wavelength views of these topics, our perspective is that of solar radiophysics (see also [2] for recent reviews and discussions in the context of the FASR[6]

[3] Reuven Ramaty High-Energy Solar Spectroscopic Imager (space observatory)
[4] Very Large Array (Socorro, New Mexico)
[5] Nobeyama Radio Heliograph (Nobeyama, Japan)
[6] Frequency-Agile Solar Radiotelescope (in development)

program). We have organized some of the new material from CESRA 2004 in these areas into sections on new observational constraints (Section 2, dealing with new X-ray and radio inputs), on particle acceleration and propagation (Section 3), and on radio emission mechanisms (Section 4).

The essence of the radio observational technique lies in its ability to sense the presence of energetic electrons remotely by a variety of emission mechanisms.

Particle acceleration frequently accompanies the coronal restructuring involved in a flare or a coronal mass ejection (CME), and general consensus holds that multiple kinds of particle acceleration are at work. Radio astronomers have also observed for years the production of suprathermal electrons in association with active regions even in the absence of flares (e.g., metric type I noise storms). With radio techniques we can perform imaging spectroscopy over a many-decade span of the frequency spectrum, observing free-free continuum, plasma emissions or synchrotron radiation. The exciting thing now is to place these remote particle observations into the context of the plasma motions and heating observed at other wavelengths, and to relate them quantitatively to the coronal magnetic field. The association with solar energetic particles (SEPs) as observed *in situ* also has become a more important undertaking as the imaging and magnetographic data improve in quality. Radio observations in the future will indeed contribute substantially to our understanding of the solar corona.

Only a handful of radio observatories currently have imaging multi-frequency observational capability and are devoted to continuous solar observation. Others have occasional programs of solar observation. The VLA and the GMRT[7] are examples of the latter, and we hope that ALMA[8] will be another in the future. Table 1 summarizes some of the currently-available observational capabilities in the radio domain. The radio spectrum is vast and the available facilities highly specialized in many cases. We apologize for the sketchiness of Table 1, which really ought to be replaced by a four-dimensional graphic (spatial resolution, temporal resolution, spectral resolution, polarization capability).

Future major new solar-dedicated observing facilities (specifically FASR and the Chinese Solar Radioheliograph) will greatly extend the table of capabilities. Furthermore the importance of flare observations in the mm-submm range, as described below in Section 2.2, strongly motivates observations with better spatial resolution, possibly with ALMA. The existing SST[9] will be upgraded to perform observations in the sub-millimeter domain at 850 GHz and in the near infrared (7-14μ, or 21.5-43 THz). A new concept for space observations has also been proposed to carry far-infrared observations (35 and 150μ, or 2 and 8.6 THz) together with γ-ray observations (MIRAGES; [5]).

[7] Giant Metrewave Radio Telescope (Pune, India)
[8] Atacama Large Millimeter Array (in development)
[9] Solar Submillimeter Telescope (El Leoncito, Argentina)

Table 1. Solar radio astronomy: current capabilities of solar-dedicated instruments

Range	Image resolution	Time resolution	Spectral resolution
submm	Few′ (SST)[a]	1 ms	Fixed frequencies 212 GHz-405 GHz
mm	Few″ (NoRH)	1 s	Fixed frequencies 17 GHz-34 GHz
cm	10″ (NoRH)	50 ms	Few % 1-18 GHz (OVRO[b])
dm/m	∼1′ (NRH[c])	125 ms	5-10 frequencies 150-450 MHz

[a]Centroiding, rather than true imaging
[b]Owens Valley Radio Observatory [3]
[c]Nançay Radio Heliograph [4]

These new capabilities will greatly strengthen the quantitative interpretation of many observational properties currently known only morphologically and will surely lead to great progress.

Finally, we note the crucially important space-borne observations at EUV, X-ray, and γ-ray wavelengths. SOHO[10], TRACE[11], and RHESSI figure prominently in the list of currently-operating spacecraft with broad capabilities. RHESSI provides high-resolution γ-ray spectroscopy, as well as imaging, and higher-resolution spectroscopic hard X-ray observations are also now becoming available also from SMART-1 [6] and GSAT-2 [7] at lower energies. Imaging spectroscopy at high resolution is also possible in principle with microcalorimeter arrays, which have already been deployed in space for non-solar observations (e.g., [8]). Solar X-ray astronomers should take note and apply these techniques, with high-resolution imaging, to solar observations as well.

2 Some new observational constraints

2.1 Hard X-rays

Microflares

Flare occurrence generally follows a power law in total energy, as approximately shown in a wide variety of observations (e.g., [9]). The nomenclature is confusing; "microflare" refers to a tiny but otherwise undistinguished solar flare with total energy on the order of 10^{26} ergs – one millionth of a major flare at 10^{32} ergs. "Nanoflare" on the other hand refers to a different physical process, hypothesized by Parker [10] to explain coronal heating in terms of ubiquitous tiny non-thermal energy releases. The nanoflares, on this interpretation, would have an occurrence distribution function so steep that individual

[10] SOlar Heliospherical Observatory (space observatory)
[11] TRansition Region And Coronal Explorer (space observatory)

events would not be individually recognizable. Thus one could not observationally distinguish flares/microflares from nanoflares, except statistically or indirectly from their consequences. From other perpectives there appears to be a continuous spectrum of flares of all magnitudes. Figure 1 (left) shows that RHESSI microflare locations strongly tend to occur in active regions. Figure 1 (right) shows RHESSI thermal parameters for a similar sample of events, revealing higher temperatures (or smaller emission measures) than obtained from X-ray emission-line spectroscopy [11].

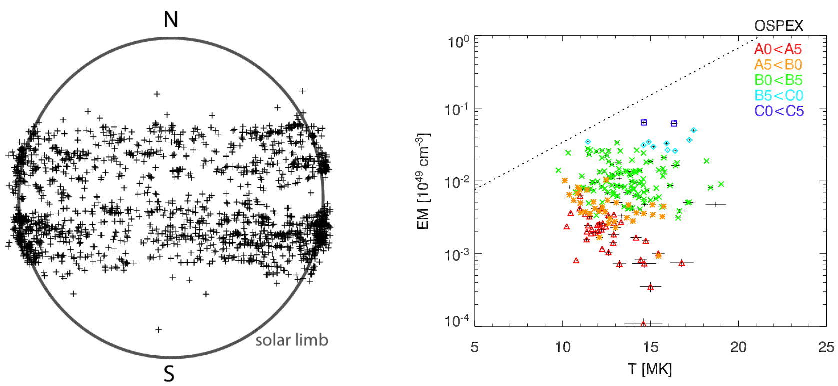

Fig. 1. *Left:* A map of RHESSI microflare positions, taken from an early 3-month sample. *Right:* Emission measure vs temperature for a smaller sample [11]; the dotted line shows the general correlation for flares [12].

For the first time for such small events, RHESSI can trace the hard X-ray spectrum to photon energies of a few keV, well below the commonly-assumed low-energy cutoff at 20-25 keV. Because the spectrum is a soft power law, this means larger total energies than might be expected for these weaker events. The non-thermal energies of these tiniest events are surprisingly large even given a possible RHESSI bias towards higher temperatures (Figure 1, right [12]), which could imply that the RHESSI thermal source contains only a fraction of the emission measure for the smaller events.

Ribbon behavior

The Hα flare ribbons (which contain the hard X-ray footpoints) mark the photospheric/chromospheric boundary of the flare's magnetic flux tubes (see the cartoon in Figure 2 [13]). This type of sketch adequately reveals the connectivity of the flare loops but does not describe the open fields linking the flare to the large-scale corona and solar wind, upon which SEPs must travel. Many variants of this "CSHKP" cartoon[12] have been published, and we generically

[12] Carmichael, Sturrock, Hirayama, and Kopp-Pneuman

call them "the reconnection model" here. This model is essentially motivated by the observations and provides a framework for discussion of eruptive or quasi-eruptive flares (e.g., [14]), but the theories remain more descriptive than predictive at present.

In the thick-target model for flare energetics the 10-100 keV electrons dominate the flare energy release, and we can trace their presence not only with hard X-rays but also (at higher resolution) with the UV and EUV imaging by TRACE [15, 16]. These observations show that the footpoints consist of bright kernels of emission with small spatial scales. This illustrates the complexity of the different scales involved in a flare/CME event; recent observations have tied the impulsive phase of the solar flare with the acceleration phase of a CME [17, 18].

Radio observations have not given us much information about the flare footpoint regions themselves, owing to absorption (free-free or gyrosynchrotron self-absorption) in the overlying flare and surrounding active-region atmosphere. At submillimeter wavelengths we do not have so much absorption but angular resolution thus far is relatively poor; we discuss new discoveries here in Section 2.2 below.

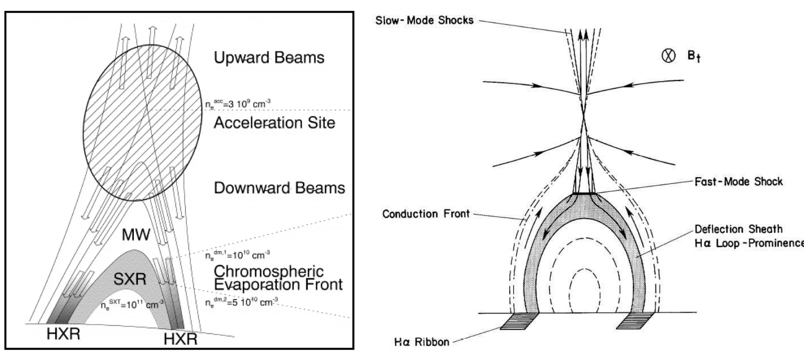

Fig. 2. Cartoon scenarios for magnetic reconnection in solar flares (*left*, from [13]; *right*, from [19]). The two views show essentially the same geometry, but the right-hand shows various shock waves that may form and be important for particle acceleration.

The key observational evidence for a model such as that of Figure 2 lies in the behavior of the ribbons (seen in Hα and many other wave bands) and hard X-ray footpoints of the closed coronal magnetic loops. The footpoints indeed reflect the ribbon structure in that the hard X-ray sources are embedded in the ribbon regions ([20, 21, 22]). However it is puzzling that these hard X-ray footpoints often only appear as a pair of compact sources with much smaller extent than the Hα ribbons themselves. The outer edges of the expanding flare ribbons should have broad line profiles as a result of the energy release envisioned in the standard model (e.g., [23]); these footpoint regions should show the "explosive" evaporation driven by non-thermal electrons closely associated with the dynamics of the reconnection. Given the time variability observed in X-rays, new estimations of Hα line profiles and energy deposition as a function of depth resulting from time-modulated high-energy power law electron beams are being developed (e.g., Varady et al., this workshop).

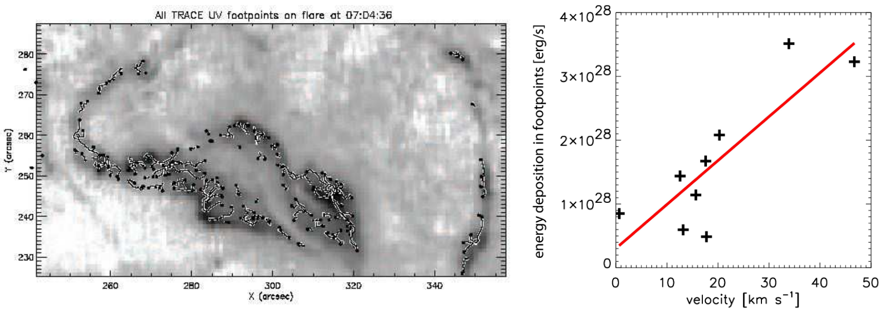

Fig. 3. *Left*: TRACE image of an M8.5 flare on 17 July 2002, showing the locations of UV bright points (footpoint sources) embedded in the ribbon structures. Several UV footpoints can exist simultaneously, and they move regularly through the ribbon envelope with a tendency to reflect magnetic features ([16]). *Right*: Correlation between apparent footpoint velocity and hard X-ray flux for the flare of 23 July 2002.

The impulsive-phase emissions of a solar flare appear throughout the spectrum, via different emission mechanisms often related to non-thermal particles. These emissions typically correlate well temporally (e.g., [15] for the example of the Bastille Day flare of 14 July 2000), but their spatial behavior differs. Figure 3 (left) shows how the UV footpoint sources behaved in an M8.5 flare observed by TRACE on 17 July 2002; this reveals many simultaneous sources that move within the ribbons. In contrast to this, the typical pattern of hard X-ray emission consists of a single dominant footpoint in each ribbon, which often moves along the ribbon as the flare progresses ([24]; [21]). This difference in image morphology has not been explained and seems inconsistent with the usual thick-target model by which we identify the Hα ribbon and hard X-ray footpoint sources as the result of energy deposition by particles accelerated in the corona.

The apparent motions of hard X-ray footpoints sometimes appear to be consistent with the expectation from the cartoons (e.g., Figure 2) in that they separate with time. Such a relationship has been sought in several studies, with varying degrees of success. In fact the majority of events display footpoint motions parallel to the ribbon elongation [24, 15, 25, 22, 26], rather than perpendicular to it. RHESSI observations have however shown a convincing correlation of properties expected in the magnetic reconnection model, illustrated in Figure 3 (right), for the X-class flare of 23 July 2002 (see also [22]).

In the model, the coronal magnetic field not only contains the energy to be released (in the form of excess $B^2/8\pi$), but also guides the energy (in the form of fast particles) into the footpoints of the coronal magnetic loops that contain the released energy. However the majority of events show footpoint motions parallel [27] to the ribbons and in various senses, behavior not explainable in a 2D cartoon representation.

Evidence of current sheets

A series of RHESSI flares observed in April 2002 suggests some further confirmation of the reconnection model, while at the same time revealing unexpected behavior. We illustrate the first of these two points in Figure 4, based upon the events described by Sui et al. [28, 29]. The left panel shows contours from three narrow bands in the range 6-20 keV, with double coronal sources apparently stretched out in the radial direction. The higher-energy (hence hotter) sources are the innermost pairs of contours. The authors interpret this phenomenon as a hot and dense current sheet forming in the corona above the flare loops, following the idea originally proposed by Syrovatskii (e.g., [30]). Such a current sheet would be a reasonable expectation for the reconnection model (Figure 2), except that present-day theory cannot predict the temperature or density of the reconnecting structure. The right panel of Figure 4 shows height-vs-time plots of loop-top and coronal sources. The coronal source – the upper anchor of the current sheet – initially remains stationary, even during the intense energy release of the impulsive phase of the flare, while the loop-top source unexpectedly moves downward (see [31] for an additional example of this behavior). These observations seem to contradict the reconnection model, which associates energy release directly with plasmoid eruption (e.g., [32]), but they could be generally consistent with the need to extract energy from the coronal magnetic field [33].

The newer observations of coronal sources can be compared with the well-known *Yohkoh* observation of the "Masuda flare" [34], in which a hard X-ray source appeared above the soft X-ray loop top during the impulsive phase of a flare on 13 January 1992. This single observation gave a great deal of momentum towards the acceptance of the reconnection model, but the new RHESSI data on the behavior of coronal sources do not generally follow this pattern. Instead of a single non-thermal "Masuda" source, one sees paired coronal thermal sources in the events of Figure 4. Coronal non-thermal sources do occur in the RHESSI data but in different configurations (e.g., [18, 35, 36]) that have not yet been systematized.

Thick-target coronal sources

The same (Figure 4) series of flares displayed an interesting hard X-ray behavior, as described by Brown (this Workshop): the RHESSI data imply that the corona itself can be dense enough to stop non-thermal electrons, thus

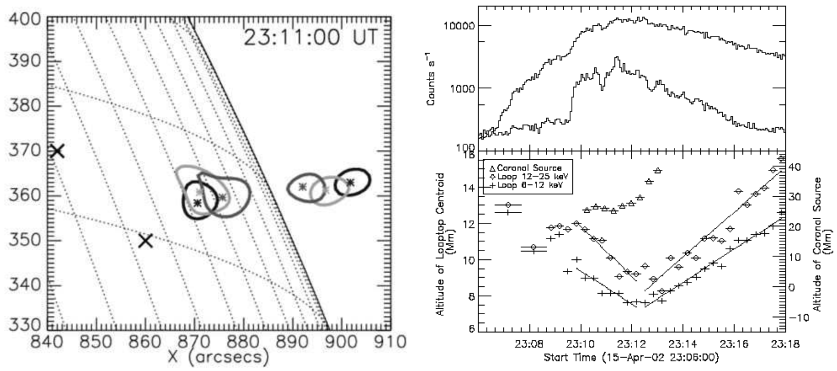

Fig. 4. RHESSI observations of apparently thermal hard X-ray sources in a flare of 15 April 2002. The panel at the left shows the footpoints of the main flare loop as +'s, while the contours show X-ray emission in three narrow bands in the range 6-20 keV (see [28]). The panel on the right shows the source motions, which reveal an unexpected *downwards* motion of the loop-top source during the initial phases of the flare.

leading to a "coronal thick target hard X-ray non-thermal source" observed up to 25 keV with little or no emission from the footpoints ([36]; see also [37, 38]). This behavior would result from emission by non-thermal electrons in a high-density loop consistent with the one deduced from the soft X-ray emission measure. The usual assumption, based on standard semi-empirical models of the solar atmosphere, would be that the electrons should penetrate to the chromosphere before losing their energy to collisions. This assumption may still be true in most cases, but the interpretation of these flares suggests that the loops may have become too dense for this to happen. We can speculate that in such cases the electron acceleration may take place in a relatively high-density coronal region.

2.2 Radio observations

Meter-centimeter domain

The extended flare of 2003 Nov. 3 provides an excellent example of the manner in which the new data can describe a complicated flare/CME event (see the right panel of Figure 5). The study presented by Dauphin et al. [39] uses Nançay radioheliograph, LASCO coronagraph, and RHESSI data (cf. Maia, this Workshop; Vršnak, this Workshop). The development of this flare/CME puts it in the category of "extended events", in which major coronal disturbances appear some time after the initial impulsive development of the flare. The time variation of this flare observed above 100 keV by RHESSI presents two broad series of bursts separated by a period of 4 minutes in which only X-ray emission below 100 keV is observed. The first part of the X-ray emission is as usual associated in the dm/m domain with type-III-like bursts. The second part (after 09:57 UT) is mainly associated with a strong continuum emission in the whole range from 2 GHz to almost 200 MHz. A decimetric/metric type II emission is observed between the two parts of the hard X-ray emission starting at an unusual high frequency of 600 MHz. A fast (1420 km/s) coronal mass ejection is observed by the LASCO coronagraph on SOHO.

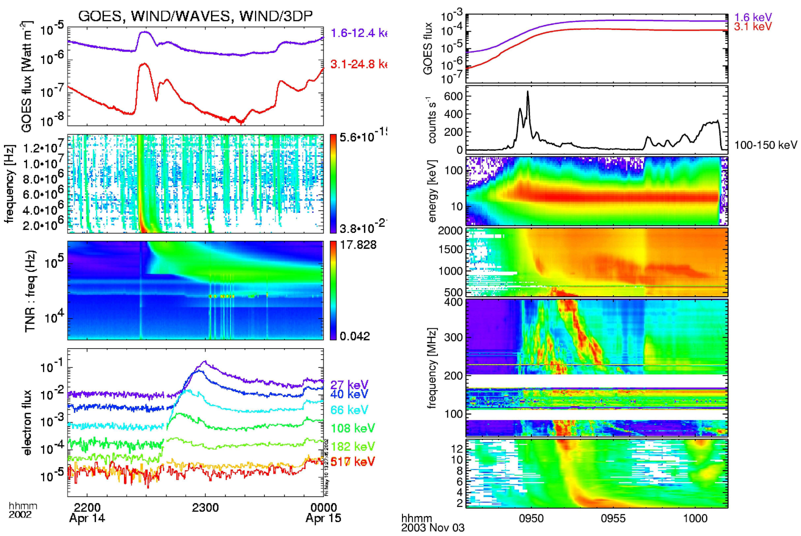

Fig. 5. *Left* Type III burst and interplanetary electron event; *right* from top to bottom: Time evolution of the GOES X-ray flux and of the X-ray RHESSI counts in the 100-150 keV energy band, RHESSI X-ray spectrogram, radio composite spectrum observed between 2 GHz to 1 MHz by PHENIX-2 (ETH Zürich), OSRA (AIP Potsdam) and the WIND/WAVES experiment. Note the continuum enhancement at 09:57 UT corresponding to the second phase of energy release observed in hard X-ray wavelength range [39]; (Krucker, this Workshop).

In this event, the "extended" phase begins extremely suddenly, at approximately 09:57 UT (Figure 5, right); the onset crosses many wavebands (from 200 MHz through 89 GHz [39] and into the hard X-rays). The observations suggest that gyrosynchrotron emission is the prevailing emission mechanism even at decimetric wavelengths for the broad-band radio emission. The simultaneity of this broad-band is much sharper than typical CME time scales, limited by the local Alfvén speed or some low multiple of it, and strongly suggests non-thermal particles as the coronal energy transport in this case. RHESSI can image the HXR sources in both phases, as shown in Figure 6. They are dominated by footpoints above 50 keV just as in the impulsive phase (see also [40]) ; these data establish that "extended flares" also have dominant footpoint emission in hard X-rays despite their strong coronal effects. However, the footpoint separation is larger in the late phase, as is the extent of the 20-25 keV source. The link with the CME onset should be further examined.

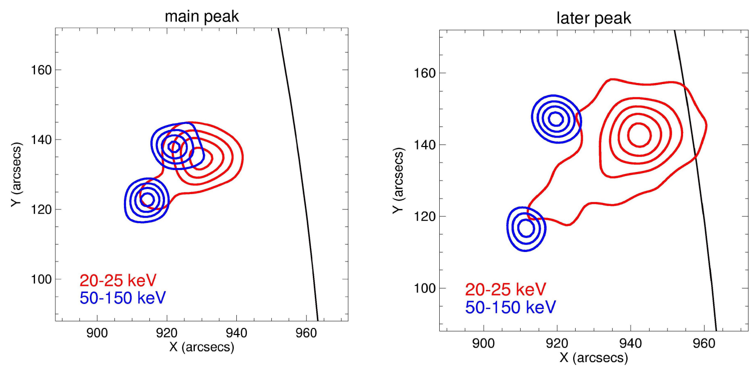

Fig. 6. RHESSI images of the early and late phases of the 2003 Nov. 3 event (Krucker, this Workshop; see also [39]).

A new observing window for flares: mm to submm

Submillimeter observations of flares (presented by Lüthi and by Trottet) provide new diagnostics for analyzing high energy electrons in solar flares. Indeed if emitted by gyrosynchrotron emission they require ultrarelativistic electrons ($>$ few MeV) to explain them. Thus such data point to the most extreme particle acceleration processes. Prior to this millennium, however, no *submillimeter* and few mm-wave observations of flares had been reported (e.g., [41]). We now have independent submillimeter observations of flares from two observatories: the SST at El Leoncito in Argentina [42] and the Köln Observatory for Submillimeter and Millimeter Astronomy (KOSMA) at Gornergrat in Switzerland [43]. The instruments use substantially different techniques, combining those of radio and infrared astrononomy. The higher frequency at El Leoncito, 405 GHz, corresponds to a wavelength of 740 μ, and an additional atmospheric window occurs at about half that wavelength. The SST is being upgraded to perform there (850 GHz) and in the far infrared (7-14 μ or 43-21.5 THz) (Trottet et al., this Workshop). The increasing opacity of the terrestrial atmosphere as one goes to short wavelengths, due largely to water vapor, makes it essential to observe from a high, dry site with adequate spatial reference to cancel out the atmospheric fluctuations (e.g., [44]). The large quiet-Sun brightness at high frequencies also implies the use of an interferometric or spatially chopping scheme for background cancellation.

The opening of the new spectral windows above 200 GHz for solar flares has provided some unexpected results. The spectral upturn seen at the highest

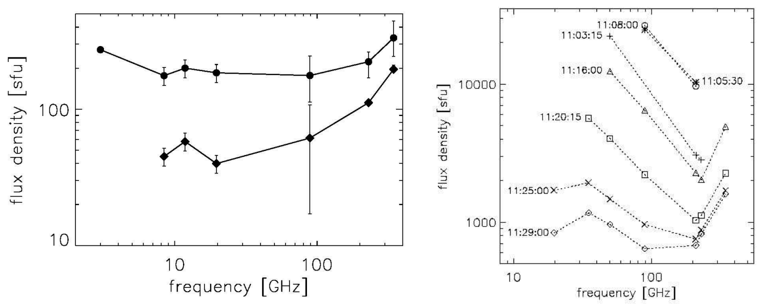

Fig. 7. Microwave/submm spectra from (*left*) an X2.1 flare on 12 April 2001, observed with the KOSMA telescope on Gornergrat [43], and (*right*) an X1.7 flare on 28 October 2003 [45]. The spectra show a surprising increase at the highest frequencies (230 and 345 GHz), inconsistent with a thermal source or with the extension towards high frequencies of the optically thin part of the gyrosynchrotron emission observed below 100 GHz.

frequencies (212 and 405 GHz at El Leoncito [42]; 230 and 345 GHz at Gornergrat [43]), as seen in the flux-density spectrum (Figure 7, is not consistent with an optically thin thermal source, nor with the high-frequency extension of the optically-thin gyrosynchrotron emission of energetic electrons observed below 100 GHz. Likewise the increase is inconsistent with synchrotron self-absorption if non-thermal. For thermal emissions, we are thus likely to be viewing thermal sources not physically located in the solar corona, but rather in denser atmospheric layers (see [46]). If this is the case, then substantial new theoretical work will be required. We speculate that the RHESSI results on the 0.511 MeV γ-ray line width [47] also require a new treatment of the lower solar atmosphere during flare conditions, especially in view of the recent discovery of near-IR emission from flares [48]. In the case of nonthermal emissions, the > 200 GHz emission may arise from optically-thick synchrotron emission from relativistic electrons in a source different from the one emitting at low frequencies, free-free emission from the chromosphere due to energy deposited by electrons or protons or by synchrotron emission from pion-decay positrons. This last process, first described by Lingenfelter and Ramaty [49] could be reconsidered for the high frequency observations given the possible observation of π_0-decay γ-rays from flares showing a spectral increase above 200 GHz.

Imaging in the submillimeter domain remains limited, by diffraction, to the arc-minute resolutions. However both the El Leoncito and Gornergrat observations involve multiple feeds, providing for crude image centroiding and size determination [50, 45]. The flare centroids are determinable with arc-second resolution and may show systematic apparent motions, as seen in the examples of Figure 8.

As the right side of Figure 8 suggests, the centroid locations for a major limb flare occurred at low altitudes. This image localization reinforces the idea

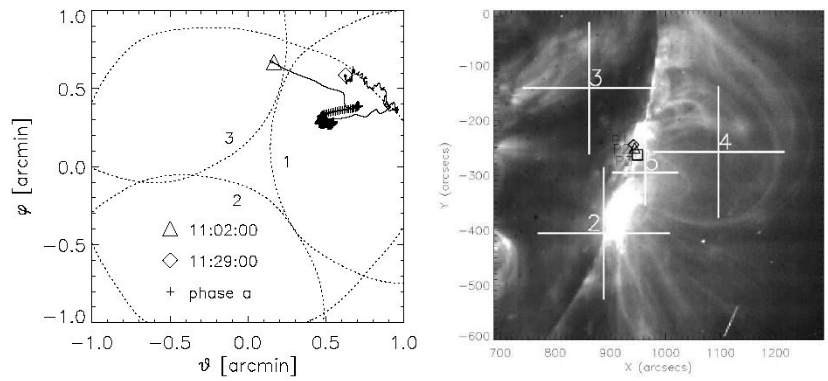

Fig. 8. *Left*: source positioning for the flare of 28 October 2003 during different periods of the flare [45], showing the layout of the multiple feeds of the KOSMA telescope. *Right*: source positioning by SST for the flare of 4 November 2004 [42]; the large crosses show the mapping of the feed locations on a TRACE image, and the symbols show centroid locations for different phases of the flare.

derived from the spectral turn-up that the THz emission is concentrated in the low atmosphere. Note however that this flare was characterized by dense coronal loops that were bright enough to appear in white light even projected against the dark sky [51], and if the submm sources included a coronal contribution the centroid locations might need re-interpretation. Higher angular resolution at mm and submm wavelengths, with true imaging, would therefore help to clarify the nature of the new spectral component.

Lastly the time variability of the new mm-wave sources also may offer some new surprises. The El Leoncito observations appear to show rapid (100-500 msec) modulations [42]. These modulations could in principle reflect an intermittent energy release best visible at the highest particle energies (hence the shortest wavelengths in the synchrotron spectrum). Figure 9 (left) shows an example of this kind of variability.

Ejecta and fine structures

The event of 2003 November 3 (Section 2.2) was also an eruptive event, and the ejecta could be followed by several instruments in the low corona [52]. We still have no theoretical consensus on the reason for the coronal loss of equilibrium that produces a coronal mass ejection, but current data have shown it to be closely related in time to the impulsive phase of the associated flare [17] when observable. The RHESSI event of 2002 April 21 and 2002 July 23 provide well-observed RHESSI examples of ejective flares [18, 35].

Now decimetric spectrographs show a class of emissions know as "drifting pulsating structures (DPS)," which can be imaged in hard X-rays (e.g., [53]). These sources reflect plasmoid ejection and may be associated at met-

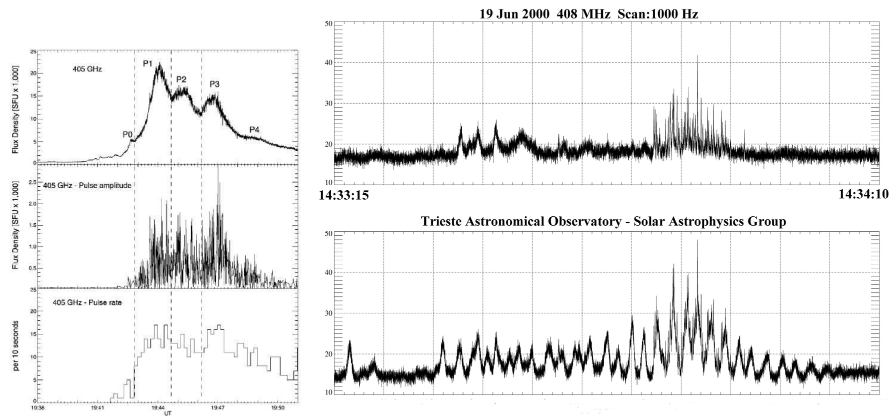

Fig. 9. *Left:* Rapid variability detected at the highest frequency observed at El Leoncito for the flare of 4 November 2004 [42]. The panels, from top to bottom, show the flux, the pulse amplitude, and the pulse rate. *Right:* Example of extremely fast variations at 408 MHz in observations from the Trieste Solar Radio System (Magdalenič, this Workshop).

ric wavelengths with type II radio bursts. Karlický (this Workshop) proposes that such structures map the magnetic field reconnection responsible for the flare energy release, and furthermore that the decimetric time variability (the pulsations) correspond with reasonable time scales for bursty reconnection. Figure 10 shows an example, with good time coincidence between DPS occurrence, plasmoid ejection, and hard X-ray emissions. Super-fast structures have also been reported with characteristic time scales of a few tens of ms and narrow bandwidth around 10 MHz in the dm wavelength range (Figure 9, right) (Magdalenič, this workshop). They probably reveal intermittent energy release and are preferentially observed around 600 MHz in the frequency range which could be imaged with future instruments such as FASR or a forthcoming Chinese solar radioheliograph.

3 Acceleration and propagation mechanisms

As stated by Burgess (this Workshop), "Collisionless shocks are a key component in astrophysical systems to transfer bulk flow kinetic energy to a small population of highly energetic particles and it is a truth universally acknowledged that shocks are effective particle accelerators." Shocks in many configurations are indeed often cited to explain various populations of non-thermal particles observed in the interplanetary medium and in the corona in connection with flares and CMEs. The universal role of electron acceleration by shocks has however been questioned (e.g., [54, 57]) concerning the real efficiency of such a mechanism to produce flare energetic electrons interacting at

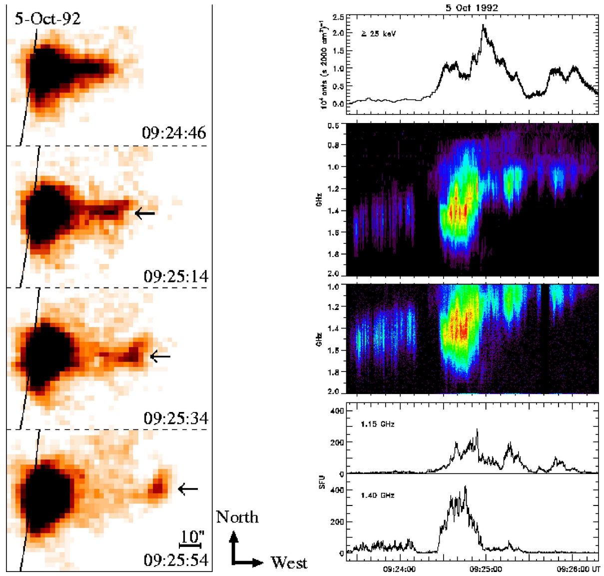

Fig. 10. Drifting pulsating structures (DPS) of 5 October 1992 observed in *Yohkoh* SXT soft X-ray images *(left)* and with the Ondřejov spectrograph *(right)*. The upper panel shows BATSE hard X-rays >25 keV.

the Sun for the impulsive-phase hard X-ray emission. Flares pose indeed an especially difficult problem for acceleration theory, since so much energy must be tied up in accelerated electrons (as confirmed by RHESSI observations [35, 55]), and even more interestingly, also in the accelerated ions responsible for γ-ray emissions [56] (as also confirmed by RHESSI observations of e.g. the 23 July 2002 event [35]). It could be difficult to invoke shock acceleration with so high an efficiency in this context, so that other mechanisms also must be considered. Relativistic particle acceleration of escaping particles can also occur in the corona far from the flare site, not in connection with the CME shock and not coincident in time with the impulsive phase. How would a large-scale shock be created and efficiently accelerate particles in such a circumstance?

The traditional "thick target" model envisions a "black box" acceleration site in the low corona, related in one way or another to magnetic reconnection, from which beams of electrons stream up and down and produce radio and HXR emissions preferentially. These electrons have a power-law spectral distribution that may extend into the γ-ray energy range. There is substantial uncertainty about the location of the "black box" and also about whether the acceleration properties can be easily disentangled from particle propagation effects (viz., the currently developing "collapsing trap" ideas [58, 30, 59, 60]). This is one of the reasons why studying flare ribbon development, searching for evidence of current sheets, and observing thick-target coronal sources (Section 2.1) is so crucial. Brown (these Proceedings) provides a modern view of this model and notes directions in which it may be changing based on new features observed by RHESSI. In principle an inverse-theoretical calculation can directly determine the nature of the source electron energy distribution from the X-ray spectra [61, 62], aided greatly by the improved energy resolution RHESSI provides.

The relationship between magnetic reconnection and particle acceleration in solar flares is presently not understood. Many authors discuss direct acceleration in the current sheet (represented by the X point in Figure 2; see e.g., [63, 64, 65, 66]). Electron and proton spectra are computed and it is shown that increasing the longitudinal ("guide") magnetic field in the RCS increases the acceleration efficiency (e.g., [63]). Another interesting prediction of test-particle simulations is to show that the inclusion of a finite guide field introduces some asymmetry in the particle propagation, implying that electron numbers and spectra could be different from one footpoint to the other [64]. Changing the sign of the particle should reverse the predominant footpoint; protons and electrons could be accelerated to different footpoints as also shown by Zharkova and Gordovskyy [67]. It should be further investigated whether this effect may explain the different electron and ion interactions sites observed with RHESSI [68].

Other possibilities less directly related to the reconnection process also exist, specifically in the large-scale shock waves associated with the plasma flows (fast-mode or slow-mode, or in turbulence excited by these flows (e.g., [69] and references therein) or in their origin.

Another substantial caveat regarding discussions of particle acceleration and propagation is the distinction between a kinetic plasma theory and ideal MHD. The plasma trapped and propagating in flare loops has a well-developed non-thermal tail (evidenced by HXR and γ-ray emissions), at least during the impulsive phase, which evolves with time, space, and pitch angle. The cartoons of Figure 2 do not describe any of this. The flare magnetic structure indeed may be much more complicated, as discussed at this Workshop by L. Vlahos.

Microwave and hard X-ray observations show different aspects of the particle distribution functions during the flare evolution. In brief, electrons must stop (the thick-target model) to produce strong hard X-ray emission; gyrosynchrotron emission, however, is not an appreciable energy-loss mechanism for the hard X-ray energy range, and can persist as long as the electrons are in a strong magnetic field. Mirroring motion in a coronal trap thus enhances the microwave flux relative to the hard X-ray flux and induces a different behavior for the temporal evolution of HXR and microwave spectral indices. This trapping can be demonstrated directly via microwave radioheliograph data, as shown in Figure 11 looking at the time profiles of loop-top and foot-point sources at 17 and 34 GHz.

In spite of this progress, it has still proven difficult to relate the two populations of non-thermal electrons in the impulsive phase; the hard X-rays generally sample the spectrum at a few tens of keV in the thick target, whereas

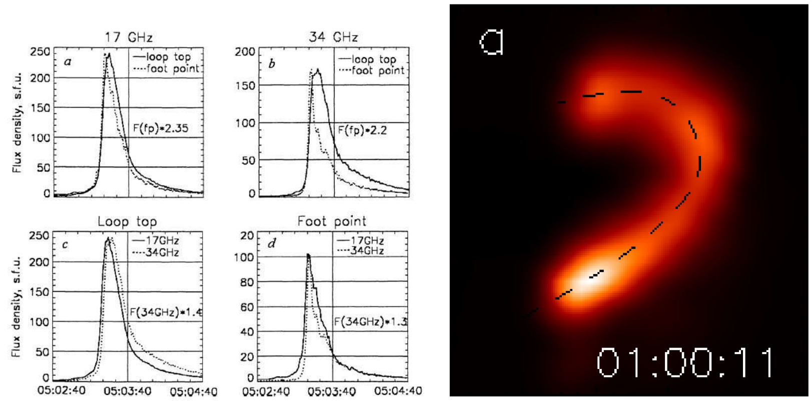

Fig. 11. *Left:* Clear evidence for trapping, derived from Nobeyama microwave observations, comparing $10'' \times 10''$ photometric boxes to obtain 17 and 34 GHz light curves at footpoint and looptop for for a flare of 13 March 2000 [70]. The delay at the looptop implies trapping. *Right:* Rise phase of a loop flare observed at Nobeyama, showing the clear presence of the footpoint sources at 34 GHz.

the microwaves sample mildly relativistic electrons typically in trapping configurations. Because of the tight time correlation between hard X-ray and microwave bursts, the two populations appear to be closely related. Nevertheless discrepancies continue to be reported (e.g., between the spectral indices deduced from the optically thin part of the gyrosynchrotron spectrum and the HXR emitting electrons [71]). The problem may lie in the simplicity of the model assumptions, even in the interpretation of the microwave spectrum [72, 73]. Another solution may lie in the spectral photon flattening observed in several flares above 500-600 keV (e.g., [74, 75]) which may easily explain why electron spectra deduced from >1 MeV gyrosynchrotron-emitting electrons are flatter than the spectra deduced at tens of keV from X-rays. Simple attempts to relate the spectral slopes of the bremsstrahlung and synchrotron-emitting electrons have indeed shown that the centimeter/millimeter-emitting electrons are related to the hard, high energy region on the HXR/γ-ray spectrum [74]. Such an interpretation could even hold for the combined observations of NoRH and RHESSI of the 23 July 2002 event, given the flattening of the HXR/GR spectrum above 500-600 keV reported by both [76] and [77].

Apart from the number of non-thermal electrons and their low energy cut-offs, microwave observations provide also information on the coronal magnetic field [78, 79]. The exploitation of the precise gyroresonance condition across an active-region corona is exciting future prospect for frequency-agile microwave imaging spectroscopy [80, 78].

What about high-energy ions? Radio techniques do not tell us much directly about their presence, but – depending somewhat upon the abundance of neon [56] – the energy content in ions may even exceed that of the electrons.

This further compromises models or theories in the MHD framework, which cannot treat these huge energies self-consistently. MacKinnon & Toner [81] comment on still greater complexities; the energy spectra of accelerated ions may differ by species in flares, as they do when observed *in situ*.

4 Radio emission mechanisms

4.1 Type III emission from electron beams

Type III bursts have been understood conceptually for some decades, but remain an interesting area of theoretical development (E. Kontar & V. Mel'nik, this Workshop). We illustrate this via the data in Figure 5 (left), which traces an event from GOES soft X-rays out through dekametric and kilometric radio signatures, all the way to the particles observed at the WIND spacecraft near one AU (and the Langmuir waves observed *in situ* there).

An electron beam, possibly produced in one of the acceleration sites sketched in Figure 2, runs out along open (type III bursts) or closed (U bursts) magnetic field lines in the corona. As the beam propagates outward, micro-instabilities result in the generation of Langmuir waves, which then couple into the electromagnetic emission that we see. The beam develops with time such that only its leading edge contributes to this process, and we see waves at the plasma frequency or its harmonic from the instantaneous position (hence density) of this moving front. Kontar & Mel'nik (this Workshop) conclude that a gas-dynamic approach can produce the spectrum of Langmuir waves explicitly, and that radio emission can further be calculated using the weak-turbulence approximation. The brightness temperature is found to depend strongly on the beam velocity. Much work remains, though, in the area of obtaining a self-consistent solution in an inhomogeneous plasma that can match the direct observations at 1 AU and also lead to an understanding of the escape of the radio emission.

4.2 Gyrosynchrotron emissions at microwave

Fleishman (this Workshop) presented improved calculations of incoherent and coherent gyrosynchrotron emissions from anisotropic electron distributions. The pitch-angle anisotropy affects the intensity and the spectral index of the emission in the optically thin region, which could explain differences in spectral indices observed fot loop-top and foot-point sources with NoRH. Mel'nikov (this Workshop) also raised the question of Razin suppression in solar centimeter-wave observations (see also [82]). With the Razin cutoff frequency $\mathrm{f}_R = 2f_p^2/3\mathrm{f}_B \sim 20\ \mathrm{n}_e/\mathrm{B}$, in cgs units, we can infer values in the range of a few GHz. In the era of full centimeter-wave imaging spectroscopy (i.e., with FASR) it seems likely that this effect will need to be considered.

5 Conclusions

The material covered in Working Group I again demonstrates how broadly significant the radio observations are in our understanding of small scale energy release, acceleration and transport of particles. It is on these small scales (not yet reachable through observations) that particle acceleration can occur. The combination of radio observations, which provide sensitive diagnostics of energetic electrons, with those from other wavelengths provides the best way to study particle acceleration. Our facilities at radio wavelengths(see Table 1) are good but still inadequate in many ways. There seem to be no real technological limits on major improvements in solar radio observations, especially from the point of view of imaging spectroscopy in the cm-mm range where scattering is not so important.

For centimeter-millimeter wavelengths, we look forward to the new facilities (including ALMA and FASR [2]) now being developed. ALMA, for example, will help in understanding the interesting new mm/submm discoveries described here. We believe that FASR will finally *solve* the problem of identifying the site of impulsive-phase particle acceleration, which remains irritatingly uncertain.

At longer wavelengths we look forward eagerly to the STEREO observations, for example, which will for the first time make 3D observations of the motions of coronal sources such as type III bursts or CMEs. The dm-m wavelengths provide the best tools for understanding the dynamics of the middle and upper corona, hard to observe but critically important for the propagation of CMEs and the acceleration of high-energy particles.

6 Acknowledgments

Hudson was supported by NASA under contract NAS5-98033 with Goddard Space Flight Center.

7 Appendix

Working group I participants:

D. Burgess, C. Dauphin, B. Dennis, L. Fletcher, G. Fleishman, R. Galloway, P. Giuliani, B. Hamilton, I. Hannah, G. Huang, H. Hudson, M. Karlický, J. Kasparova, E. Kontar, S. Krucker, T. Lüthi, A. Mackinnon, J. Magdalenič, D. Maia, P. Mallik, V. Mel'nikov, T. Neukirch, R. Schroeder, G. Trottet, M. Väänänen, M. Varady, A. Veronig, N. Vilmer, L. Vlahos, P. Wood

References

1. Klein, K.L.: Energy Conversion and Particle Acceleration in the Solar Corona. Lecture Notes in Physics **612** (2003)
2. Gary, D.E., Keller, C.U.: Solar and Space Weather Radiophysics - Current Status and Future Developments. Eds D. E. Gary & C. U. Keller, Astrophysics and Space Science Library, **314** (2004)
3. Gary, D.E., Hurford, G.J.: Coronal temperature, density, and magnetic field maps of a solar acitve region using the Owens Valley Solar Array. ApJ **420** (1994) 903
4. Kerdraon, A., Delouis, J.M.: The Nançay Radioheliograph. LNP Vol. 483: Coronal Physics from Radio and Space Observations **483** (1997) 192
5. Molodij, G., Trottet, G.: Far Infrared Telescope (TIR) Project. In: EAS Publications Series. (2005) 199
6. Huovelin, J., and 19 co-authors: The SMART-1 X-ray solar monitor (XSM): calibrations for D-CIXS and independent coronal science. PSS **50** (2002) 1345
7. Jain, R., Dave, H., Kumar, S., Deshpande, M.R.: Results of one year of observations of solar flares made by "Solar X-ray Spectrometer (SOXS)" Mission. In: COSPAR, Plenary Meeting (2005) 744
8. Kelley, R.L., and 13 co-authors: The microcalorimeter spectrometer on the ASTRO-E X-ray observatory. Nuclear Instruments and Methods in Physics Research A **444** (2000) 170
9. Hudson, H.S.: Solar flares, microflares, nanoflares, and coronal heating. Solar Phys **133** (1991) 357
10. Parker, E.N.: Nanoflares and the solar X-ray corona. ApJ **330** (1988) 474
11. Hannah, I.G., Christe, S., Krucker, S., Hudson, H.S., Fletcher, L., Hendry, M.A.: RHESSI microflare statistics. In: ESA SP-575: SOHO 15 Coronal Heating. (2004) 259
12. Feldman, U., Doschek, G.A., Behring, W.E., Phillips, K.J.H.: Electron temperature, emission measure, and X-ray flux in A2 to X2 X-ray class solar flares. ApJ **460** (1996) 1034
13. Aschwanden, M.J.: Particle acceleration and kinematics in solar flares - a synthesis of recent observations and theoretical concepts. Space Science Reviews **101** (2002) 1
14. Moore, R.L., Sterling, A.C., Hudson, H.S., Lemen, J.R.: Onset of the magnetic explosion in solar flares and coronal mass ejections. ApJ **552** (2001) 833
15. Fletcher, L., Hudson, H.: The magnetic structure and generation of EUV flare ribbons. Solar Phys **204** (2001) 69
16. Fletcher, L., Pollock, J.A., Potts, H.E.: Tracking of TRACE ultraviolet flare footpoints. Solar Phys **222** (2004) 279
17. Zhang, J., Dere, K.P., Howard, R.A., Kundu, M.R., White, S.M.: On the temporal relationship between coronal mass ejections and flares. ApJ **559** (2001) 452
18. Gallagher, P.T., Dennis, B.R., Krucker, S., Schwartz, R.A., Tolbert, A.K.: RHESSI and TRACE observations of the 21 April 2002 X1.5 flare. Solar Phys **210** (2002) 341
19. Forbes, T.G., Malherbe, J.M.: A shock condensation mechanism for loop prominences. ApJL **302** (1986) L67
20. Masuda, S., Kosugi, T., Hudson, H.S.: A hard X-ray two-ribbon flare observed with *Yohkoh*/HXT. Solar Phys **204** (2001) 55

21. Metcalf, T.R., Alexander, D., Hudson, H.S., Longcope, D.W.: TRACE and *Yohkoh* observations of a white-light flare. ApJ **595** (2003) 483
22. Krucker, S., Hurford, G.J., Lin, R.P.: Hard X-ray source motions in the 2002 July 23 gamma-ray flare. ApJL **595** (2003) L103
23. Svestka, Z.: Solar Flares, Dordrecht: Reidel, 1976 (1976)
24. Sakao, T., Kosugi, T., Masuda, S.: Energy release and particle acceleration in solar flares with respect to flaring magnetic loops. In: ASSL Vol. 229: Observational Plasma Astrophysics : Five Years of *Yohkoh* and Beyond. (1998) 273
25. Qiu, J., Lee, J., Gary, D.E., Wang, H.: Motion of flare footpoint emission and inferred electric field in reconnecting current sheets. ApJ **565** (2002) 1335
26. Asai, A., Yokoyama, T., Shimojo, M., Masuda, S., Kurokawa, H., Shibata, K.: Flare ribbon expansion and energy release rate. ApJ **611** (2004) 557
27. Bogachev, S.A., Somov, B.V., Kosugi, T., Sakao, T.: The motions of the hard X-ray sources in solar flares: images and statistics. ApJ **630** (2005) 561
28. Sui, L., Holman, G.D.: Evidence for the formation of a large-scale current sheet in a solar flare. ApJL **596** (2003) L251
29. Sui, L., Holman, G.D., Dennis, B.R.: Evidence for magnetic reconnection in three homologous solar flares observed by RHESSI. ApJ **612** (2004) 546
30. Somov, B.V.: Cosmic plasma physics. Kluwer Academic Publishers, 2000. Astrophysics and space science library ; v. 251 (2000)
31. Veronig, A., et al.: X-ray sources and magnetic reconnection in the X3.9 flare of 2003 November 3. AAp (2006)
32. Forbes, T.G.: A review on the genesis of coronal mass ejections. JGR **105** (2000) 23,153
33. Hudson, H.S.: Implosions in coronal transients. ApJL **531** (2000) L75
34. Masuda, S., Kosugi, T., Hara, H., Tsuneta, S., Ogawara, Y.: A loop-top hard X-ray source in a compact solar flare as evidence for magnetic reconnection. Nature **371** (1994) 495
35. Lin, R.P., Krucker, S., Hurford, G.J., Smith, D.M., Hudson, H.S., Holman, G.D., Schwartz, R.A., Dennis, B.R., Share, G.H., Murphy, R.J., Emslie, A.G., Johns-Krull, C., Vilmer, N.: RHESSI observations of particle acceleration and energy release in an intense solar gamma-ray line flare. ApJL **595** (2003) L69
36. Veronig, A.M., Brown, J.C.: A coronal thick-target interpretation of two hard X-ray loop events. ApJL **603** (2004) L117
37. Wheatland, M.S., Melrose, D.B.: Interpreting *Yohkoh* hard and soft X-ray flare observations. Solar Phys **158** (1995) 283
38. Fletcher, L., Martens, P.C.H.: A model for hard X-ray emission from the top of flaring loops. ApJ **505** (1998) 418
39. Dauphin, C., Vilmer, N., Lüthi, T., Trottet, G., Krucker, S., Magun, A.: Modulations of broad-band radio continua and X-ray emissions in the large X-ray flare on 3 November 2003. Advances in Space Research **35** (2005) 1805
40. Qiu, J., Lee, J., Gary, D.E.: Impulsive and gradual nonthermal emissions in an X-class flare. ApJ **603** (2004) 335
41. Croom, D.L.: Solar millimeter bursts. In: CESRA-2, Committee of European Solar Radio Astronomers. (1971) 85
42. Kaufmann, P., Raulin, J., de Castro, C.G.G., Levato, H., Gary, D.E., Costa, J.E.R., Marun, A., Pereyra, P., Silva, A.V.R., Correia, E.: A new solar burst spectral component emitting only in the terahertz range. ApJL **603** (2004) L121
43. Lüthi, T., Magun, A., Miller, M.: First observation of a solar X-class flare in the submillimeter range with KOSMA. AAp **415** (2004) 1123

44. Hudson, H.S.: The solar-flare infrared continuum - Observational techniques and upper limits. Solar Phys **45** (1975) 69
45. Lüthi, T., Lüdi, A., Magun, A.: Determination of the location and effective angular size of solar flares with a 210 GHz multibeam radiometer. AAp **420** (2004) 361
46. Ohki, K., Hudson, H.S.: The solar-flare infrared continuum. Solar Phys **43** (1975) 405
47. Share, G.H., Murphy, R.J., Smith, D.M., Schwartz, R.A., Lin, R.P.: RHESSI e^+-e^- Annihilation radiation observations: implications for conditions in the flaring solar chromosphere. ApJL **615** (2004) L169
48. Xu, Y., Cao, W., Liu, C., Yang, G., Qiu, J., Jing, J., Denker, C., Wang, H.: Near-infrared observations at 1.56μ of the 2003 October 29 X10 white-light flare. ApJL **607** (2004) L131
49. Lingenfelter, R.E., Ramaty, R.: On the origin of solar flare microwave radio bursts. PSS **15** (1967) 1303
50. Raulin, J.P., Kaufmann, P., Olivieri, R., Correia, E., Makhmutov, V.S., Magun, A.: Time and space distribution of discrete energetic releases in millimeter-wave solar bursts. ApJL **498** (1998) L173
51. Leibacher, J.W., Harvey, J.W., Kopp, G., Hudson, H., GONG Team: Remarkable low-temperature emission of the 4 November 2003 limb flare. American Astronomical Society Meeting **204** (2004)
52. Dauphin, C., Vilmer, N., Krucker, S.: Observations of soft X-ray rising loops associated with a type II and CME emission in the large X-ray flare on 3 November 2003. AAp (2006)
53. Khan, J.I., Vilmer, N., Saint-Hilaire, P., Benz, A.O.: The solar coronal origin of a slowly drifting decimetric-metric pulsation structure. AAp **388** (2002) 363
54. Klein, K.L., Trottet, G.: The Origin of solar energetic particle events: coronal acceleration versus shock wave acceleration. Space Science Reviews **95** (2001) 215
55. Emslie, A.G., Dennis, B.R., Holman, G.D., Hudson, H.S.: Refinements to flare energy estimates: A followup to "Energy partition in two solar flare/CME events" by A. G. Emslie et al. Journal of Geophysical Research (Space Physics) **110** (2005) 11,103
56. Ramaty, R., Mandzhavidze, N., Kozlovsky, B., Murphy, R.J.: Solar atmopheric abundances and energy content in flare-accelerated Ions from γ-ray spectroscopy. ApJL **455** (1995) L193
57. Klein, K.L., Schwartz, R.A., McTiernan, J.M., Trottet, G., Klassen, A., Lecacheux, A.: An upper limit of the number and energy of electrons accelerated at an extended coronal shock wave. AAp **409** (2003) 317
58. Brown, J.C., Hoyng, P.: Betatron acceleration in a large solar hard X-ray burst. ApJ **200** (1975) 734
59. Karlický, M., Kosugi, T.: Acceleration and heating processes in a collapsing magnetic trap. AAp **419** (2004) 1159
60. Giuliani, P., Neukirch, T., Wood, P.: Particle motion in collapsing magnetic traps in solar flares. I. kinematic theory of collapsing magnetic traps. ApJ **635** (2005) 636
61. Piana, M., Massone, A.M., Kontar, E.P., Emslie, A.G., Brown, J.C., Schwartz, R.A.: Regularized electron flux spectra in the 2002 July 23 solar flare. ApJL **595** (2003) L127

62. Kontar, E.P., Emslie, A.G., Piana, M., Massone, A.M., Brown, J.C.: Determination of electron flux spectra in a solar flare with an augmented regularization method: Application to RHESSI data. Solar Phys **226** (2005) 317
63. Hamilton, B., McClements, K.G., Fletcher, L., Thyagaraja, A.: Field-guided proton acceleration at reconnecting X-points in flares. Solar Phys **214** (2003) 339
64. Hamilton, B., Fletcher, L., McClements, K.G., Thyagaraja, A.: Electron acceleration at reconnecting X-points in solar flares. ApJ **625** (2005) 496
65. Dalla, S., Browning, P.K.: Particle acceleration at a three-dimensional reconnection site in the solar corona. AAp **436** (2005) 1103
66. Efthymiopoulos, C., Gontikakis, C., Anastasiadis, A.: Particle dynamics in 3-D reconnecting current sheets in the solar atmosphere. AAp **443** (2005) 663
67. Zharkova, V.V., Gordovskyy, M.: Particle acceleration asymmetry in a reconnecting nonneutral current sheet. ApJ **604** (2004) 884
68. Hurford, G.J., Schwartz, R.A., Krucker, S., Lin, R.P., Smith, D.M., Vilmer, N.: First γ-ray images of a solar flare. ApJL **595** (2003) L77
69. Miller, J.A., Cargill, P.J., Emslie, A.G., Holman, G.D., Dennis, B.R., LaRosa, T.N., Winglee, R.M., Benka, S.G., Tsuneta, S.: Critical issues for understanding particle acceleration in impulsive solar flares. JGR **102** (1997) 14,631
70. Mel'nikov, V.F., Reznikova, V.E., Yokoyama, T., Shibasaki, K.: Spectral dynamics of mildly relativistic electrons in extended flaring loops. In: ESA SP-506: Solar Variability: From Core to Outer Frontiers. (2002) 339
71. White, S.M., Krucker, S., Shibasaki, K., Yokoyama, T., Shimojo, M., Kundu, M.R.: Radio and hard X-ray images of high-energy electrons in an X-class solar flare. ApJL **595** (2003) L111
72. Fleishman, G.D., Mel'nikov, V.F.: Optically thick gyrosynchrotron emission from anisotropic electron distributions. ApJ **584** (2003) 1071
73. Fleishman, G.D., Mel'nikov, V.F.: Gyrosynchrotron emission from anisotropic electron distributions. ApJ **587** (2003) 823
74. Trottet, G., Vilmer, N., Barat, C., Benz, A., Magun, A., Kuznetsov, A., Sunyaev, R., Terekhov, O.: A multiwavelength analysis of an electron-dominated gamma-ray event associated with a disk solar flare. AAp **334** (1998) 1099
75. Vilmer, N., Trottet, G., Barat, C., Schwartz, R.A., Enome, S., Kuznetsov, A., Sunyaev, R., Terekhov, O.: Hard X-ray and γ-ray observations of an electron-dominated event associated with an occulted solar flare. AAp **342** (1999) 575
76. Smith, D.M., Share, G.H., Murphy, R.J., Schwartz, R.A., Shih, A.Y., Lin, R.P.: High-resolution spectroscopy of γ-ray lines from the X-class solar flare of 2002 July 23. ApJL **595** (2003) L81
77. Share, G.H., Murphy, R.J., Skibo, J.G., Smith, D.M., Hudson, H.S., Lin, R.P., Shih, A.Y., Dennis, B.R., Schwartz, R.A., Kozlovsky, B.: High-resolution observation of the solar positron-electron annihilation line. ApJL **595** (2003) L85
78. White, S.M.: Radio measurements of coronal magnetic fields. In: ESA SP-596: Chromospheric and Coronal Magnetic Fields. (2005)
79. Huang, G., Zhou, A., Su, Y., Zhang, J.: Calculations of the low-cutoff energy of non-thermal electrons in solar microwave and hard X-ray bursts. New Astronomy **10** (2005) 219
80. Bastian, T.S., Benz, A.O., Gary, D.E.: Radio emission from solar flares. ARAA **36** (1998) 131
81. Toner, M.P., MacKinnon, A.L.: Do fast protons and α particles have the same energy distributions in solar flares? Solar Phys **223** (2004) 155

82. Klein, K.L.: Microwave radiation from a dense magneto-active plasma. AAp **183** (1987) 341